This is a peer reviewed version of the following article: J. Mat. Chem. C 2017, 5, 350, which has been published in final form at http://pubs.rsc.org/en/content/articlelanding/2017/tc/c6tc04463h#!divAbstract

Charge Transport in Highly Ordered Organic Nanofibrils: Lessons from Modelling

Ganna Gryn'ova,[★†] Adrien Nicolaï,[★‡] Antonio Prlj,[†] Pauline Ollitrault,[†] Denis Andrienko,[§] Clemence Corminboeuf*[†]

[†] *Institut des Sciences et Ingénierie Chimiques, École polytechnique fédérale de Lausanne, CH-1015 Lausanne, Switzerland*

[‡] *Laboratoire Interdisciplinaire Carnot de Bourgogne, UMR 6303 CNRS-Univ. Bourgogne Franche Comté, 9 Av. A. Savary, BP 47 870, F-21078 Dijon Cedex, France*

[§] *Max Planck Institute for Polymer Research, Ackermannweg 10, 55128 Mainz, Germany*

* E-mail: clemence.corminboeuf@epfl.ch

★ These authors contributed equally.

Abstract (50-250 words)

H-aggregates featuring tight π-stacks of the conjugated heterocyclic cores represent ideal morphologies for 1D organic semiconductors. Such nanofibrils have larger electronic couplings between the adjacent cores compared to the herringbone crystal or amorphous assemblies. In this work, we show that for a set of seven structurally and electronically distinct cores, including quaterthiophene and oligothienothiophenes, the co-planar dimer model captures the impact of the monomer's electronic structure on charge transport, but more advanced multiscale modelling, featuring molecular dynamics and kinetic Monte-Carlo simulations, is needed to account for the packing and disorder effects. The differences in the results between these two computational approaches arise from the sensitivity of the electronic coupling strength to the relative alignment of adjacent cores, in particular the long-axis shift between them, imposed by the oligopeptide side chains. Our results demonstrate the dependence of the performance of H-aggregates on the chemical nature of the cores and the presence of the side chains, as well as the limitations in using the simple dimer model for a rapid computational pre-screening of the conjugated cores.

This is a peer reviewed version of the following article: J. Mat. Chem. C 2017, 5, 350, which has been published in final form at http://pubs.rsc.org/en/content/articlelanding/2017/tc/c6tc04463h#!divAbstract

Introduction

Small-molecule organic semiconductors can self-assemble into various supramolecular morphologies, from one-dimensional π-stacks to three-dimensional crystalline solids. Their charge transport properties are, among other molecular descriptors, intimately related to the weighted overlap between the orbitals, participating in the charge transfer reaction (diabatic states). The latter depends on both the electronic configuration of single molecules and their mutual position/orientation within a given macroscopic assembly.[1] For one-dimensional crystalline packing motifs, the largest charge carrier mobility could be expected for the perfectly cofacial π-stacks (Figure 1),[2] which, however, are challenging to achieve due to the inter-core Pauli repulsion.[3] H-aggregates are promising candidates in this respect as they feature slightly shifted co-parallel π-stacks.[4] Indeed, H-aggregates of the quaterthiophene and perylene diimide cores display mobilities (p- and n-type, respectively) which are 1-2 orders of magnitude higher than those of the corresponding J-aggregates.[5] Nonetheless, in most cases, bare π-conjugated cores favour the herringbone packing (see Figure 1), which maximises the number of attractive C–H···π interactions.[6] Yet, several strategies exist to impose the face-on π-stacking. Certain bare cores, e.g. with three fused thiophenes and/or with sickle,[7] circular[8] and propeller[9] shapes, form columnar stacks with the herringbone packing (see Table S1 in the Supporting Information). However, H-aggregates, which involve side chain substituents, e.g. halogen atoms, alkyl and aryl chains, hydrogen-bonding groups (e.g., peptides), etc.[10-16] enforce vertical alignment of tightly packed π-stacked cores, leading to long 1D nanowires (nanofibrils).[17] These highly-ordered morphologies are less prone to a detrimental 'bottleneck effect' that is due to small structural and energetic fluctuations, which create traps for transferring the charge along a bare π-stack and can severely impair mobility in 1D assemblies.[18,19] Effectiveness of this strategy is evidenced by the superior charge transport performance of H-aggregates of tetracene, perylene diimide and quaterthiophene compared to their non-substituted crystalline and randomly dispersed analogues.[20-22]

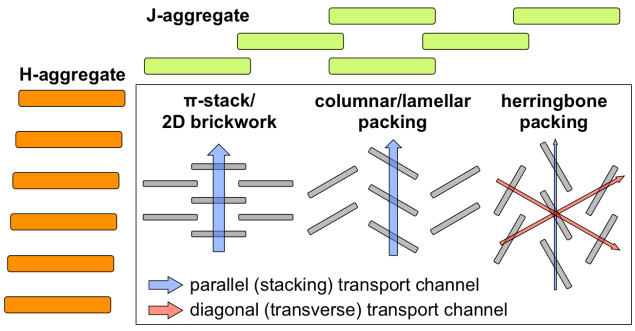

Figure 1. Typical aggregates and crystal packing motives of the π-conjugated cores. 1-column

Moreover, H-aggregates represent an ideal test case for the simplest *in silico* model of charge transport – a single co-parallel dimer. Highly ordered nanofibrils, stabilised by the side chain aggregators, feature a distinct packing motif (π-stacked core pairs), therefore their charge transport properties could (potentially)be derived from the simulations of cofacial dimers, paving a way to a swift computational pre-screening of the H-aggregates. The significance of such assessment is particularly apparent considering that the coplanar dimer is generally an inadequate approximation to other types of macroscopic assemblies. Specifically, reliable dimer-based predictions of 2D and 3D materials involve computing transfer integrals for several dimer geometries so as to account for the specificity of molecular packing (Figure 1) and thus require pre-existing knowledge of the crystal structure.[23,24,25] This approach also assumes an ideal, disorder-free assembly and is therefore not applicable to amorphous systems. An alternative *multiscale* approach, which combines molecular dynamic (MD) modelling of the nanoscale material morphology and kinetic Monte-Carlo (kMC) simulation of the charge dynamics,[26] presumably affords a truly *ab initio* description of the hopping transport[18,27,28] in organic semiconductors. Yet, this level of accuracy comes at a significant computational cost and complexity. Importantly, the aforementioned computational techniques utilise the semi-classical Marcus-Hush theory of the charge transfer under an assumption of the hopping transport mechanism.[29] Admittedly, it deduces the charge transfer phenomena to a simple set of transitions between the localised states separated by barriers and its relative importance (*vs.* the band transport) is debated in the literature.[30] Nonetheless, the Marcus-Hush model affords an excellent agreement with the experimental hole mobilities for the thin films and single-molecule crystals of various acene- and thiophene-based compounds.[31]

In the present work we focus on the *p*-type transport in H-aggregates featuring hydrogen bonding oligopeptide side chains, flanked onto the thiophene-based cores[32,33] and their oxygen analogues (Figure 2). We demonstrate that the computationally inexpensive dimer-based approach captures only some of the key trends in one-dimensional charge transport in these highly ordered nanofibrils and that a more sophisticated multiscale modelling is ultimately necessary to reach the quantitative accuracy. By comparing and contrasting the results from the two modelling strategies, we elucidate the intricate relationships between the chemical nature of the cores, their mutual alignment, controlled by the side chains, and charge transport characteristics of the investigated H-aggregates. We find that it is the electronic structure of the cores and the specifics of material's assembly rather than the disorder in it that primarily dominate the charge carrier mobility in one-dimensional nanofibrils. These findings form the basis for the design principles for the future development of new organic H-aggregate semiconductors.

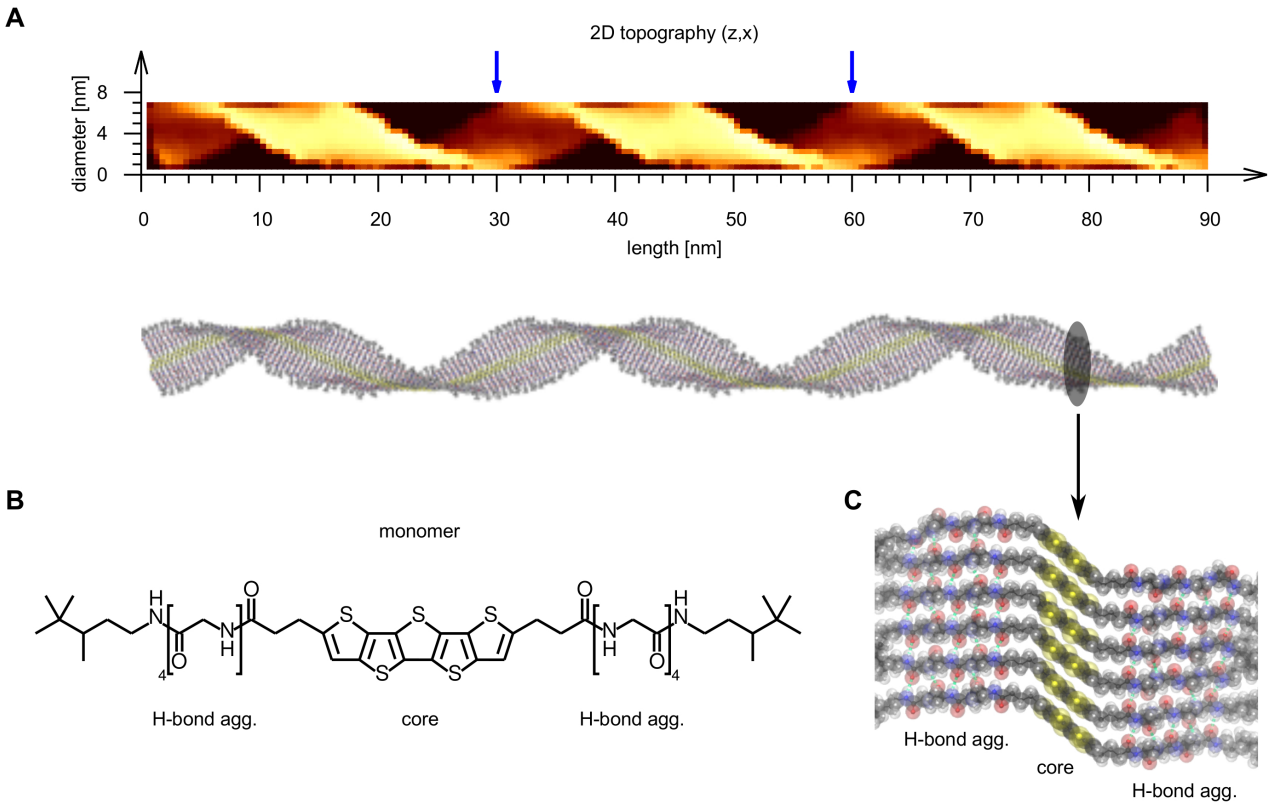

Figure 2. (A) 2D topography and atomic structure of a nanofibril made of PTA cores and oligopeptide side chains with a periodicity of 30 nm. The structure shown here corresponds to the final structure of the corresponding MD run (See Figure S4 and Table S7 in the Supporting Information). (B) Chemical structure of the H-bonding aggregators comprised of four alanine residues, flanked to the PTA core. (C) Close-up of the nanofibril, shown in panel A, illustrating π-stacked shifted PTA cores and H-bonded aggregators. 2-column

Results

Multiscale modelling. We have computed the hole transport properties of seven nanofibrils aggregated by the H-bonding side chains (Figure 2) using the multiscale approach that combines classical molecular dynamics simulations with kinetic Monte Carlo method (see Computational Details section below). Our results reveal a number of trends in both the geometric and hole transport characteristics, shown in Figure 3 and Table 1.

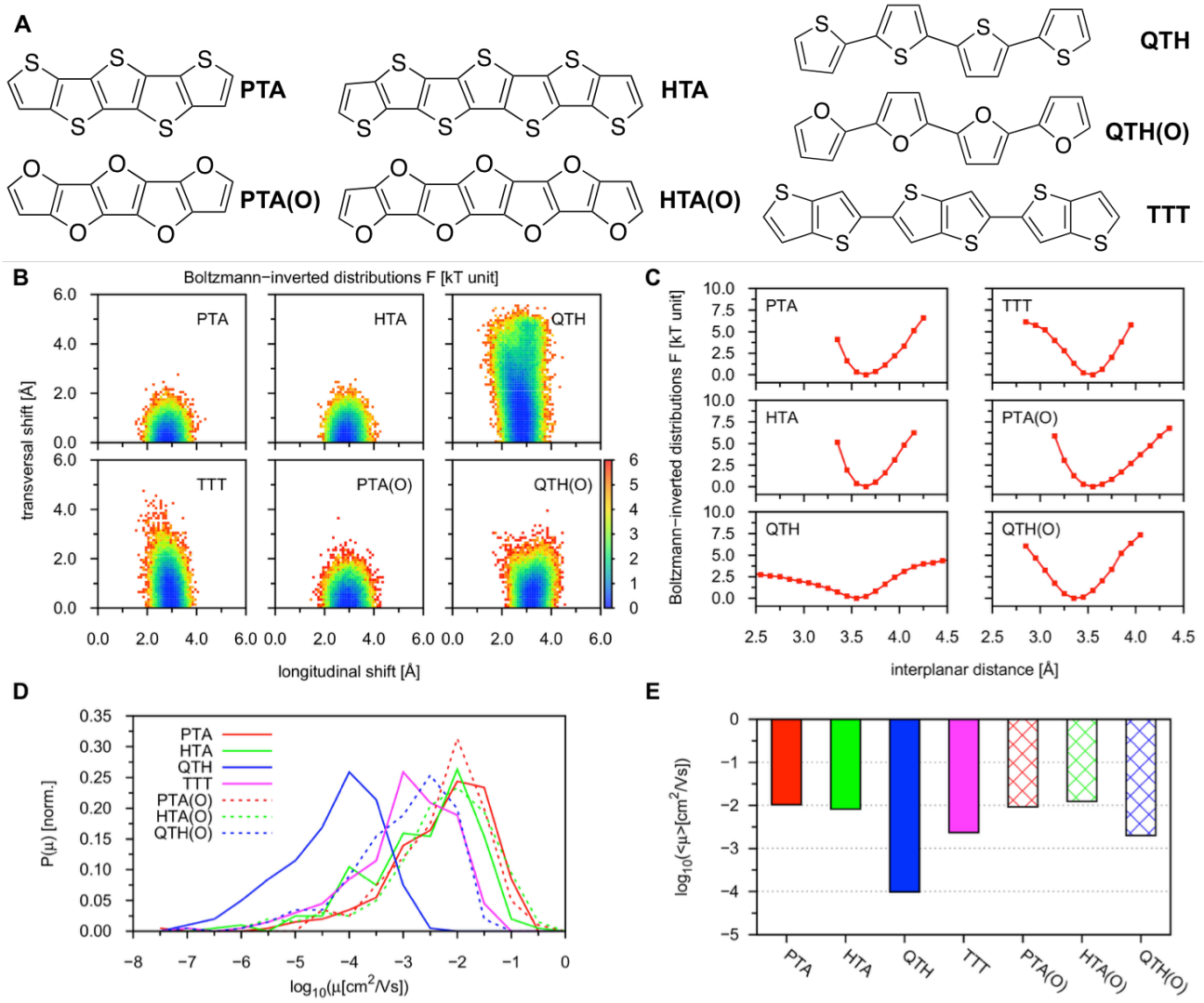

Figure 3. O- and S-containing π-conjugated cores, studied in this work. Boltzmann-inverted distributions of longitudinal and transversal shifts (B) and interplanar distances between consecutive cores of a fiber computed from all-atom MD simulations (C). (D) Probability distribution functions of mobilities μ. (E) Averaged over 200 snapshots mobilities <μ>. 2-column

Structural trends. In a nanofiber the chemical nature of the cores barely influences the longitudinal shift between the consecutive units (Figure 3A), since the side chain aggregators impose persistent alignment of the cores. The transversal shift is more sensitive to the nature of the cores, with flexible cores, such as QTH and TTT, exhibiting shifts as large as 5 Å and 3 Å, respectively, and the rigid fused cores showing much less pronounced short-axis displacements. The most probable value for all studied systems is around 0-1 Å and is imposed by the side chains. These H-bonding aggregators also control the intercore distances, as seen in the corresponding energy profiles, all featuring similar minimum distances (Figure 3B). Oxygen-containing compounds show systematically smaller (0.1-0.2 Å) π-stacking distance as compared to compared

to their sulphur analogues. Another distinction is the noticeably flatter profiles for the most floppy QTH cores. This is a direct consequence of their large transversal shift (Figure 3A), as small π-stacking distances are typically coupled with large transversal shifts.[34]

Mobility trends. As shown in Figure 3D, the probability distribution functions of mobilities are fairly similar in width and height for all studied aggregates, indicating that the nanofibril dynamics and thermal fluctuations brought by the MD simulations in the TECE solvent at 300 K are comparable in all runs. In addition, energetic and configurational disorders included in CT calculations (see Figure S8 in the Supporting Information) are similar for all the studied systems, confirming that the disorder is not the main reason for their diverse performances. The mean of such distribution reflects the charge mobility of a corresponding nanofibril (Table 1). Fibrils, built of floppy QTH cores perform worse than both the less flexible TTT and rigid QTH(O). TTT-based fibrils are intermediate between PTA/HTA and QTH. Overall, nanofibers containing fused PTA and HTA cores exhibit the largest charge mobilities, whereas fibers based on floppy QTH cores perform the worst. Mobility of the nanofibrils composed of larger hexathienoacene cores is essentially the same as that of the pentathienoacene-based nanofibrils. Finally, replacement of sulphur by oxygen atoms in the fused cores has no appreciable effect on mobility despite shortening the π-stacking distance (Figure 3D).

Table 1. Computed longitudinal and transversal shifts, interplanar distances *d* and averaged mobilities $\langle\mu\rangle$ from MD and CT simulations of the different nanofibrils, characterised by their core nature and periodicity *P*. 1-column

core	*P*, nm	shift, Å		*d*, Å	$\langle\mu\rangle$, $cm^2V^{-1}s^{-1}$	$\log_{10}\langle\mu\rangle$
		long.	trans.			
PTA	30	2.7	0.0	3.6	$1.04\ 10^{-2}$	-1.98
PTA(O)	30	2.9	0.2	3.5	$9.29\ 10^{-3}$	-2.03
HTA	60	2.8	0.1	3.6	$8.27\ 10^{-3}$	-2.08
HTA(O)	30	2.8	0.1	3.5	$1.25\ 10^{-2}$	-1.90
QTH	120	2.7	1.1	3.5	$9.79\ 10^{-5}$	-4.01
QTH(O)	75	3.2	0.2	3.3	$2.02\ 10^{-3}$	-2.69
TTT	60	2.9	0.3	3.5	$2.35\ 10^{-3}$	-2.63

Dimer-based computations. In parallel to multiscale simulations, we have estimated the hole transport properties for the investigated oxygen- and sulphur-containing π-conjugated cores in conjunction with their optimised dimer geometries (Table 2).

Table 2. Computed reorganisation energies λ_+, effective hole transfer integrals V_+, hopping rates k_+, hole mobilities μ_+, DORI compactness indices, interplanar distances d, longitudinal and transversal shifts in the PBE0-dDsC/def2-SVP optimised dimer geometries. 2-column

Core	λ_+, eV	V_+, eV	k_+, s^{-1}	μ_+, $cm^2V^{-1}s^{-1}$	DORI index [a]	d, Å	shift, Å	
							long.	trans.
				cofacial				
QTH	0.34	0.11	1.4×10^{13}	0.307	0.75	3.31	1.41	0.84
QTH(O)	0.28	0.02	9.1×10^{11}	0.019	0.54	3.26	1.36	0.55
TTT	0.33	0.19	4.3×10^{13}	0.922	0.93	3.33	1.44	0.66
PTA	0.31	0.29	1.3×10^{14}	2.653	0.69	3.28	1.88	0.04
PTA(O)	0.30	0.16	4.6×10^{13}	0.906	0.48	3.18	1.58	0.03
HTA	0.28	0.33	2.3×10^{14}	4.778	0.97	3.28	1.82	0.02
HTA(O)	0.29	0.20	7.8×10^{13}	1.524	0.67	3.17	1.27	0.02
				antifacial				
QTH		0.22	5.4×10^{13}	1.181	n/a	3.37	0.20	1.39
QTH(O)		0.03	1.7×10^{12}	0.033	0.61	3.16	0.07	1.03
TTT		0.05	2.5×10^{12}	0.053	n/a	3.34	1.13	0.24
PTA		0.37	2.2×10^{14}	4.679	0.69	3.33	0.29	0.04
PTA(O)		0.17	5.2×10^{13}	1.031	0.48	3.21	0.75	0.22
HTA		0.40	3.4×10^{14}	7.173	0.98	3.31	0.14	0.05
HTA(O)		0.22	8.9×10^{13}	1.762	0.66	3.19	0.62	0.09

[a] In several species, the intermolecular DORI domains with 0.95 isovalue are merged with the intramolecular S–S domains, hence the compactness indices for these domains cannot be compared to the rest of the systems and therefore are not reported.

Due to the symmetry of the studied monomers, two variants of dimer geometry, called disordermers,[35] need to be considered – cofacial and antifacial (see Figure 6A). First, we examine the correlation (quantified by the square of the correlation coefficient, R^2) between the properties of the co- and antifacial disordermers: 0.93 for the transport rate and hole mobility, 0.97 for the DORI compactness index and 0.58 for the interplanar distance. The disordermers are most noticeably

dissimilar for the QTH and TTT cores, but are very close for the oligothienoacene and oligofuroacene cores. Therefore, the average transport properties of a given H-aggregate of the fused-core monomers would not be affected greatly if either the co- or the antifacial dimer pairs were dominant. This is particularly useful since it is problematic to control this mutual core arrangement in practice. Noteworthy, in the classical MD simulations the nanofibrils are built from cofacial π-stacks, hence the following discussion of the dimer-based transport properties will also focus on the cofacial dimers.

Secondly, heteroaromatic π-conjugated cores, investigated here, can be broadly split into three classes based on the dependencies of their transport rates on the reorganisation energies and effective transfer integrals (Figure 4A):[36]

1) sulphur-containing cores with 'floppy' C–C single bonds between the rings (QTH, TTT) are characterised with high reorganisation energies, average transfer integrals and, correspondingly, relatively low hole transport rates (~10^{13} s^{-1}) and mobilities;
2) fused S-containing cores with high transfer integrals, low reorganisation energies and, accordingly, the best transport characteristics (k_+ over 10^{14} s^{-1}). Larger intermolecular overlap area grants higher mobility of the heptathienophene core compared to pentathienophene;
3) oxygen-containing analogues of the previous group, (PTA(O), HTA(O)) have the lowest λ_+ values but also moderate transfer integrals, resulting in moderate transport characteristics (k_+ ~10^{14} s^{-1}).

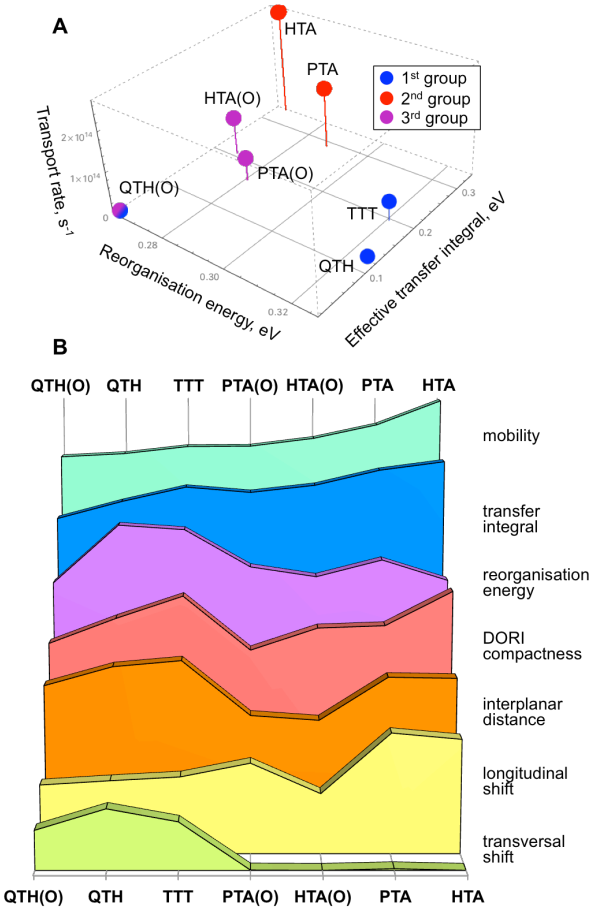

Figure 4. (A) 3D plot of the computed transport rates, reorganisation energies and effective transfer integrals. (B) Relative trends in the normalised computed dimer-based structural and transport properties for the cofacial dimers of the investigated cores. *y*-Axis is qualitative only. 1-column

In this dimer-based approach, geometries of the bare monomer assemblies were fully relaxed, leading to some variability in the structural parameters (Figure 4B). While the longitudinal shift in dimers featuring flexible cores is relatively constant, it varies noticeably in the fused-core systems; the opposite trend is observed for the short-axis displacement. Obtained trend in mobilities generally follows the transfer integral values, with slight deviations observed in the systems with significantly differing reorganisation energies. Tendencies in the transport characteristics also largely mirror those in the DORI compactness indices. Interestingly and in contrast to the *multiscale* modelling results, larger HTA and HTA(O) cores afford somewhat higher mobility than the smaller PTA and PTA(O) analogues. Furthermore, the O-containing fused cores have lower electron compactness indices and transfer integrals despite shorter inter-monomer distances, as compared to the sulphur-containing analogues. Consequently, mobilitites of PTA and HTA are higher than those of PTA(O) and HTA(O), respectively.

Discussion

We have modelled charge transport in several 1D nanofibrils featuring O- and S-containing π-conjugated cores, flanked with oligopeptide side chains (Figure 5). Investigated nanofibrils exemplify a realistic system featuring single mutual arrangement of the cores – tight cofacial π-stack with relatively constant intercore distances and translational shifts, imposed by the hydrogen-bonding side chains. On the other hand, fully optimised dimers of the bare cores lack this geometry constraint and thus correspond to the mutual alignment of two cores, most beneficial in energy (rather than the frontier orbital overlap[22a]) and dictated by their chemical structure. Correspondingly, certain similarities as well as differences exist between the results of the two computational approaches (Figure 5).

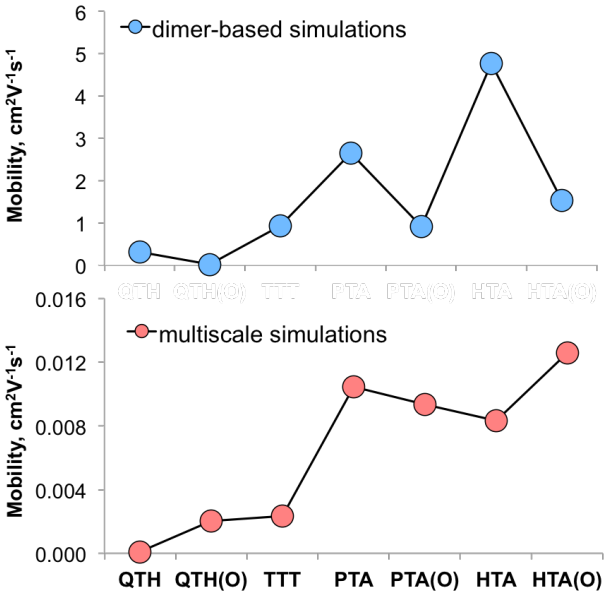

Figure 5. Comparison of the hole mobility values, computed using dimer-based and multiscale approaches. 1 column

Analysis of these relationships reveals the factors that ultimately determine the charge transport characteristics of the studied organic semiconducting 1D cofacial aggregates:

• Floppy heteroatomatic cores, such as QTH and TTT, are deplanarised when isolated and neutral due to low barriers for rotation around their C–C single bonds and related weak conjugation between the aromatic rings. However, upon charging these cores tend to flatten thus resulting in high reorganisation energies.[37] This leads to low mobilities even despite high inter-monomer electron overlaps (DORI indices) and average transfer integrals (Figure 4B). Substituting sulphur with oxygen atoms flattens and stiffens the neutral core, significantly lowering the reorganisation

energies, as evident for the QTH(O) core. However, the dimer-based charge mobility of QTH(O) is still unimpressive due to low transfer integral of the dimer in the optimised, longitudinally shifted geometry (see Figure S1 in the Supporting Information). On the contrary, in a nanofibril the side chain H-bonding aggregators modify the longitudinal displacement, rectifying the performance of the QTH(O) core. This highlights the improvement in the transport properties that can be achieved by a targeted choice of the aggregator and thus the displacement it imposes.[38]

• From the multiscale point of view, larger π-conjugated cores (HTA(O) and HTA) do not directly result in electronic couplings and mobilities higher than those of the smaller cores (PTA(O) and PTA). This is consistent with both the experimental measurements[39] and computations on oligoacene cores.[40] However, transfer integrals and mobilities of larger π-conjugated cores from the dimer-based computations are consistently higher than the corresponding values of the smaller cores. This disparity originates in non-equal longitudinal shifts in the optimised dimers and is in fact resolved in the dimers with zero longitudinal shifts.[41]

• Arguably, the most striking qualitative deviation between the outcomes of two computational models is the comparative performance of fused S- *vs* O-containing cores (Figure 5). According to the dimer-based approach, S-containing cores have systematically better charge transport characteristics (despite larger inter-monomer distances) than the oxygen analogues, while in the multiscale simulations their performance is comparable. The likely origin of this phenomenon is that the species, containing more diffuse and more polarisable sulphur atoms, benefit from the charge penetration effect,[42] whilst their oxygen analogues do not (see Figure S3 in the Supporting Information).[43,44] In the dimers of the S-containing cores there exists an optimal value of lateral shift, at which their charge penetration, orbital overlaps and, consequently, charge transfer integrals are maximised. PTA(O) and HTA(O) cores containing more compact oxygen atoms lack this effect. However, in the nanofibrils this subtle effect and the associated distinction in the transport properties between the S- and O-containing heteroacenes are effectively supressed as a consequence of H-bonding side chain aggregators, larger intercore separation and structural fluctuations. Therefore, such delicate quantum-chemical design principles are not necessarily transferrable from the simple dimer models to the realistic macro assemblies.

The dissimilarities between the 1D nanofibrils and their dimer models arise almost exclusively in the differing arrangements (and, in particular, the longitudinal shifts) of the neighbouring cores – effectively fixed by H-bonding side chain aggregators in a nanofibril as opposed to fully relaxed and dictated by the core's nature in the optimised dimers. In addition, the dimer-based mobilities are systematically higher than the multiscale and experimental ones by several orders of magnitude

due to the abovementioned bottleneck effect.[18,19] Overall, the dimer-based method, which does not require any pre-existing knowledge of the macromolecular assembly, reveals the impact of the electronic structure of the cores on the transport properties of the structurally controlled nanofibrils. However, the multiscale modelling is necessary to account for the side chains, disorder and packing effects. Ultimately, in some of the studied systems these factors dominate the observed mobility trends, thus illustrating the limitations of using the coplanar dimer model as a tool for rapid pre-screening of the monomer cores for the highly ordered H-aggregates.

Conclusions and Implications

We have characterised the charge transport properties of several π-conjugated heteroaromatic cores, highly ordered into 1D nanofibrils by means of H-bonding side chain aggregators, using multiscale and dimer-based computational approaches. Side chain aggregators, introduced to enforce the π-stacking and minimise the dynamic fluctuations, impose a characteristic longitudinal shift between the adjacent π-stacked cores within the fibril, which in turn influences their electronic coupling strength. In the optimised dimers this structural feature is determined by the interplay of various components of the interaction energy (electrostatic, Pauli repulsion, dispersion, charge penetration) and is different for the chemically dissimilar cores. However, these subtle quantum-chemical effects largely vanish in the investigated 1D nanofibrils, in which the longitudinal shift is instead fixed at a fairly constant value of ~3Å by the side chain aggregators, as opposed to a relatively broad spectrum of shifts in the bare core dimers. This observation provides a useful design principle of selecting the side chain aggregators that ensure the most beneficial (in terms of electronic coupling) alignment of the cores.

The charge transport properties, assessed using the computationally cost-effective dimer model, should be interpreted with care: While this method does capture the impact of the monomer structure, it is limited to systems that consist of the co-parallel π-stacked cores. More complex morphologies, such as 2D and 3D crystals and conjugated polymers, cannot be reduced to a single unit and call for more diverse and system-specific models. Even in the highly ordered π-stacked H-aggregates, the dimer approximation could fail whenever other factors dramatically affect the charge transport. Thus, multiscale modelling is still imperative to obtain quantitatively accurate transport measures for both the highly ordered 1D nanofibrils and more evolved assemblies. This method goes beyond the bare chemical cores, accounting for the effects of the environment (e.g., solvent and temperature), substituents, processing conditions, and molecular packing.

Computational details

According to the Marcus-Hush theory,[29] the hole transport rate, k, can be evaluated as

$$k = \frac{4\pi^2}{h}\frac{1}{\sqrt{4\pi\lambda k_B T}}V^2 \exp\left[-\frac{(\Delta E-\lambda)^2}{4\lambda k_B T}\right], \quad \textbf{Eq. 1}$$

where λ is the reorganisation energy, V is the electronic coupling (hole transfer integral), ΔE is the site-energy difference (the driving force), h is the Planck's constant, k_B is the Boltzmann constant and T is the absolute temperature. In the simplest case of a one-dimensional lattice, the hole mobility, μ, can be evaluated using the Einstein relation[1,45]

$$\mu = \frac{D}{k_B T}, \quad \textbf{Eq. 2}$$

with the diffusion constant D given by

$$D = \frac{d^2 k}{2}, \quad \textbf{Eq. 3}$$

where d is the lattice spacing. The reorganization energy and electronic coupling in Eq. 1 can be determined using quantum-chemical methods, the reorganization energy as[29]

$$\lambda = \left(E^{charge=0}_{cation\ geom.} - E^{charge=0}_{neutral\ geom.}\right) + \left(E^{charge=+1}_{neutral\ geom.} - E^{charge=+1}_{cation\ geom.}\right), \quad \textbf{Eq. 4}$$

where E are the energies, of the charged and neutral molecules in the optimised and single-point geometries. The corresponding electron coupling in a dimer, V, reads

$$V = \frac{J - S\frac{\varepsilon_1+\varepsilon_2}{2}}{1-S^2}, \quad \textbf{Eq. 5}$$

where J is the charge transfer integral, S is the overlap integral, ε_1 and ε_2 are the site energies for the hole transport.[46]

Molecular dynamic simulations. MD simulations of nanofibrils were carried out using the GROMACS software package[47,48] (version 4.6). Parameters of the cores and H-bond aggregators (ALA residues) atoms were taken from the GAFF [49] and AMBER99sb-ildn [50] force-fields, respectively. In addition, GAFF parameters for each core have been obtained using the antechamber module of AmberTools14[51] and the AM1-BCC scheme[52] was used to compute the partial charges. MD simulations of nanofibrils were performed in explicit solvent, *i.e.* 1,1,2,2-tetrachloroethane $C_2H_2Cl_4$ (TECE) [53]. The duration of each MD run is 10 ns, the time step used is 2 fs and coordinates were saved every 1 ps. MD trajectories were performed in the NVT ensemble at T = 300 K using

the velocity-rescale thermostat[54] (τ = 0.1 ps). The electrostatic term was computed using the Particle Mesh Ewald (PME) algorithm[55] and a cutoff of 1.0 nm was used for the rest of the to non-bonded interactions. Before the 10 ns production run, an energy minimisation using the conjugate gradient algorithm as implemented in GROMACS 4.6[48] and an equilibration in the NPT ensemble (T = 300 K and P = 1 bar) using the same thermostat and a Berendsen barostat[56] during 500 ps was performed. Additional details are given in the Supporting Information.

VOTCA. Charge transport (CT) computations were performed using the VOTCA software package.[57] For each of the seven nanofibrils, the CT properties were computed for 201 structures extracted from the MD simulations, from 8 to 10 ns, in time intervals of 10 ps. These structures correspond to those belonging to the most stable part of the MD trajectory (8-10 ns, evidenced by the global RMSD, see Figure S6 in the Supporting Information) and are considered as equilibrated and incorporating thermal disorder. The relaxation period observed at the beginning of each MD run is not used here. The kinetic Monte Carlo algorithm was used to compute the hole mobilities along the nanofibrils. The hopping rates were evaluated using the Marcus-Hush theory according to Eq. 1.[29] In computing the reorganisation energy, only the core part of each monomer (capped with CH_3 groups to approximate the H-bonding aggregators) was considered. The reorganisation energy, computed according to Eq. 4 at the PBE0/def2-SVP level of theory, as such omits the contribution from the so-called outer-sphere reorganisation energy (which accounts for the relaxation of the environment). The latter is expected to have similar influence on the different nanofibrils, thus not influencing the key trends.

The site-energy difference ΔE includes the contributions from the external electric field, electrostatic interactions, and polarisation effects, and can be evaluated using a perturbative treatment of solid-state interactions and polarizable force-fields.[57,58] The contribution from the externally applied electric field **F** to the total site-energy difference is

$$\Delta E^{ext} = e\,\mathbf{F}\cdot\Delta\boldsymbol{r} \qquad \textbf{Eq. 6}$$

where e is the unit charge and Δr is a vector connecting the centres of mass of the neighbouring molecules. Knowing the partial atomic charges of the neutral and charged molecules, electrostatic energy ΔE^{el} can be evaluated.[57,59] Partial charges were computed using the CHEPLG model[60] at the PBE0/def2-SVP level of theory using Gaussian 09 software package.[61] Induction effects were estimated based on the Thole model,[62] as implemented in VOTCA. The energetic disorder in the studied nanofibrils is negligible (see Figure S8 in the Supporting Information) and was included in our mobility computations.[57,63] Electronic coupling elements V were computed for each pair of the

neighbouring molecules using computationally inexpensive ZINDO semiempirical method[64] and Gaussian 09 software package.[61] The transfer integrals were evaluated based on the HOMO orbitals of the monomers (frozen core approximation).[65] The impact of the peptide side chains on the reorganisation energies and electronic couplings was assessed for selected system and was found to be insignificant (see discussion and Table S5 in the Supporting Information).

Upon evaluating the charge transfer rates between the neighbouring sites, the hole transport dynamics was performed for a single hole in a periodic box using the kinetic Monte Carlo algorithm. An external electric field of 10^7 V m^{-1} was applied along the nanofibril axis and the temperature of 300 K was assumed for both rates and dynamics. The dynamic simulation for each structure was performed with a total time of 0.001 s and the hole mobility was computed by velocity averaging. Finally, the hole mobility corresponding to each nanofibril is computed by averaging the hole mobilities of 201 structures.

Dimer-based computations. Geometries and electronic energies of the monomers were optimised at the PBE0/def2-SVP level using Gaussian 09 software package.[61] Electronic energies of the monomers and the respective cation radicals in optimised and vertical geometries, and ultimately the reorganisation energies, were computed at the same level of theory. Geometries of their parallel π-stacked dimers were optimised at the PBE0-dDsC[66]/def2-SVP level using the development version of Q-Chem.[67] The reliability of this method for modelling of the noncovalently bound systems has already been shown.[66,68] Since these systems have C_{2h} and C_{2v} symmetries, two dimer geometries (so-called disordermers[35]) were considered – co- and antifacial (Figure 6A). For all species, vibrational frequencies analysis was performed to confirm that they were the global minima on the potential energy surfaces. The hole transfer integrals were computed at the PBE0-dDsC/DZP level of theory using the projection method implemented in ADF2014[69], which utilises the orthogonalised orbitals of each monomer fragment as the basis for the dimer's Hamiltonian. The site-energy difference (ΔE in Eq. 1) was taken equal to zero since the two molecules in a dimer are identical and the effect of the environment is neglected at this stage. The computation of electronic coupling elements was complemented by the evaluation of geometrical descriptors of the dimers (Figure 6B): the charge transfer length taken as an average interplanar distance, the average transversal (along the short molecular axis) and longitudinal (along the long molecular axis) relative translational shifts between the monomers in the optimised dimer geometry. The pitch, roll and yaw tilt angles in the optimised geometries of the investigated dimers are relatively close to zero.

We have also computed the electronic compactness, based on the density overlap regions indicator (DORI),[70] to quantify the electron density overlap between the monomers in each dimer. The strength of this density overlap, which is measured by the number of electrons inside an intramolecular DORI volume, is complementary to the hole integral transfers that depend solely on the HOMO of the involved monomers. The electron densities of the studied systems were computed at the PBE0/DZP level using ADF2014.[69] The DORI analyses were performed on a fine grid with an isovalue of 0.95 using an in-house modified version of the DGrid program.[71] Finally, the energy decomposition analysis of selected dimers was performed using the symmetry-adapted perturbation theory (SAPT0)[72], complemented by the distributed multipole analyses (DMA) to elucidate the effect of 'charge penetration'.[43] Details of these computations are given in the Supporting Information.

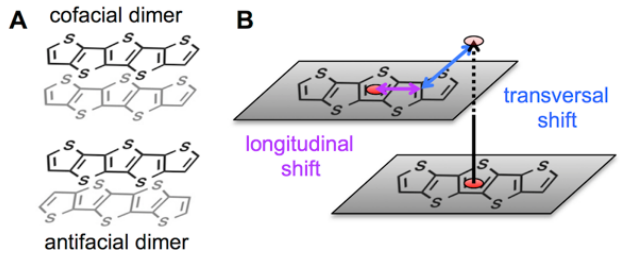

Figure 6. Mutual orientations (A) and relative displacements (B) of the monomers in an optimised dimer. 1-column

Supporting Information

Supporting Information Available: overview of mobilities, reported in the literature; complete set of computational results; details of the classical molecular dynamics and kinetic Monte Carlo simulations; Cartesian coordinates of the species in the dimer-based computations. This material is available free of charge via the Internet at http://pubs.acs.org.

Acknowledgements

The authors thank Mr Trent Parker and Prof C. David Sherrill for providing their in-house code for computing the DMA interaction energies. G.G., A.N., A.P. and C.C. acknowledge funding from the European Research Council (ERC Grants 306528, COMPOREL). D.A. thanks the BMBF grants MEDOS (FKZ03EK3503B), MESOMERIE (FKZ 13N10723), and InterPhase (FKZ 13N13661) as well as funding from the NMP-20-2014 – "Widening materials models" program under Grant

Agreement No. 646259 (MOSTOPHOS).

TOC

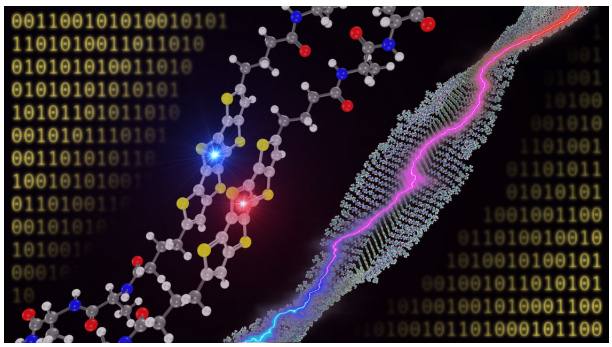

References

[1] (a) J. Cornil, D. Beljonne, J.-P. Calbert, J.-L. Brédas, Interchain Interactions in Organic p-Conjugated Materials: Impact on Electronic Structure, Optical Response, and Charge Transport. *Adv. Mater.,* 2001, **13**, 1053. (b) J.-L. Brédas, J. P. Calbert, D. A. da Silva Filho, J. Cornil, Organic semiconductors: A theoretical characterization of the basic parameters governing charge transport. *Proc. Natl. Acad. Sci. U. S. A.*, 2002, **99**, 5804. (c) V. Coropceanu, J. Cornil, D. A. da Silva, Y. Olivier, R. Silbey, J.-L. Brédas, Charge Transport in Organic Semiconductors. *Chem. Rev.,* 2007, **107**, 926.

[2] A. Bashir, A. Heck, A. Narita, X. Feng, A. Nefedov, M. Rohwerder, K. Müllen, M. Elstner, C. Wöll, Charge Carrier Mobilities in Organic Semiconductors: Crystal Engineering and the Importance of Molecular Contacts. *Phys. Chem. Chem. Phys.,* 2015, **17**, 21988.

[3] (a) C. Wand, Y. Mo, P. J. Wagner, P. R. Schreiner, E. D. Jemmis, D. Danovich, S. Shaik, The Self-Association of Graphane Is Driven by London Dispersion and Enhanced Orbital Interactions *J. Chem. Theory Comput.,* 2015, **11**, 1621. (b) S. Grimme, Do Special Noncovalent p–p Stacking Interactions Really Exist? *Angew. Chem. Int. Ed.,* 2008, **47**, 3430. (c) R. Podeszwa, R. Bukowski, K. Szalewicz, Potential Energy Surface for the Benzene Dimer and Perturbational Analysis of π-π Interactions. *J. Phys. Chem. A,* 2006, **110**, 10345.

[4] (a) F. C. Spano, C. Silva, H- and J-Aggregate Behavior in Polymeric Semiconductors. *Annu. Rev. Phys. Chem.*, 2014, **65**, 477. (b)A. Liedtke, M. O'Neill, S. M. Kelly, S. P. Kitney, B. Van Averbeke, P. Boudard, D. Beljonne, J. Cornil, Optical Properties of Light-Emitting Nematic Liquid Crystals: A Joint Experimental and Theoretical Study. *J. Phys. Chem. B*, 2010, **114**, 11975.

[5] (a) S.-o. Kim, T. K. An, J. Chen, I. Kang, S. H. Kang, D. S. Chung, C. E. Park, Y.-H. Kim, S.-K. Kwon. H-Aggregation Strategy in the Design of Molecular Semiconductors for Highly Reliable Organic Thin Film Transistors. *Adv. Funct. Mater.*, 2011, **21**, 1616. (b) Y. Che, Y. Feng, J. Gao, M. Bouvet, Self-assembled Aggregates of Amphiphilic Perylene Diimide–Based Semiconductor Molecules: Effect of Morphology on Conductivity. *J. Colloid Interface Sci.*, 2012, **368**, 387.

[6] (a) R. Bishop, Organic Crystal Engineering Beyond The Pauling Hydrogen Bond. *CrystEngComm,* 2015, **17**, 7448. (b) Y. Xiong, M. Wang, X. Qiao, J. Li, H. Li, Syntheses and Properties Of π-Conjugated Oligomers Containing Furan-Fused and Thiophene-Fused Aromatic Units. *Tetrahedron,* 2015, **71**, 852. (c) K. E. Maly, Acenes vs N-Heteroacenes: The Effect of N-Substitution on the Structural Features of Crystals of Polycyclic Aromatic Hydrocarbons. *Cryst. Growth Des.,* 2011, **11**, 5628. (d) S. Tsuzuki, K. Honda, R. Azumi, Model Chemistry Calculations of Thiophene Dimer Interactions: Origin of π-Stacking. *J. Am. Chem. Soc.*, 2002, **124**, 12200. (e) R. Biradha, M. J. Zaworotko, A Supramolecular Analogue of Cyclohexane Sustained by Aromatic C-H•••π Interactions: Complexes of 1,3,5-Trihydroxybenzene with Substituted Pyridines. *J. Am. Chem. Soc.,* 1998, **120**, 6431.

[7] R. Li, H. Dong, X. Zhan, Y. He, H. Li, W. Hu, Single Crystal Ribbons and Transistors of a Solution Processed Sickle-Like Fused-Ring Thienoacene. *J. Mater. Chem.,* 2010, **20**, 6014.

[8] J. Yin, K. Chaitanya, X.-H. Ju, Structures and Charge Transport Properties of ''Selenosulflower'' and Its Selenium Analogue ''Selflower'': Computer-Aided Design of High-Performance Ambipolar Organic Semiconductors. *J. Mater. Chem.*, 2015, **3**, 3427.

[9] Q. Xiao, T. Sakurai, T. Fukino, K. Akaike, Y. Honsho, A. Saeki, S. Seki, K. Kato, M. Takata, T. Aida, Propeller-Shaped Fused Oligothiophenes: A Remarkable Effect of the Topology of Sulfur Atoms on Columnar Stacking. *J. Am. Chem. Soc.,* 2013, **135**, 18268.

[10] (a) S. Ghosh, X.-Q. Li, V. Stepanenko, F. Würthner, Control of H- and J-Type π-Stacking by Peripheral Alkyl Chains and Self- Sorting Phenomena in Perylene Bisimide Homo- and Heteroaggregates. *Chem. Eur. J.*, 2008, **14**, 11343. (b) T. K. An, S. H. Jang, S.-O. Kim, J. Jang, J. Hwang, H. Cha, Y. R. Noh, S. B. Yoon, Y. J. Yoon, L. H. Kim, D. S. Chung, S.-K. Kwon, Y.-H. Kim, S.-G. Lee, C. E. Park, Synthesis and Transistor Properties of Asymmetric Oligothiophenes: Relationship between Molecular Structure and Device Performance. *Chem. Eur. J.*, 2013, **19**, 14052.

[11] (a) J. Mei, Y. Diao, A. L. Appleton, L. Fang, Z. Bao. Integrated Materials Design of Organic Semiconductors for Field- Effect Transistors. *J. Am. Chem. Soc.,* 2013, **135**, 6724.

[12] J. E. Anthony, Functionalized Acenes and Heteroacenes for Organic Electronics. *Chem. Rev.,* 2006, **106**, 5028.

[13] (a) H. Usta, A. Facchetti, T. J. Marks, n-Channel Semiconductor Materials Design for Organic Complementary Circuits. *Acc. Chem. Res.,* 2011, **44**, 501. (b) A. Facchetti, Semiconductors for Organic Transistors. *Mater. Today,* 2007, **10**, 28.

[14] (a) A. Nicolaï, H. Liu, R. Petraglia, C. Corminboeuf. Exploiting Dispersion-Driven Aggregators as a Route to New One-Dimensional Organic Nanowires. *J. Phys. Chem. Lett.*, 2015, **6**, 4422. (b) C. R. Medrano, M. B. Oviedo, C. G. Sánchez, Photoinduced Charge-Transfer Dynamics Simulations in Noncovalently Bonded Molecular Aggregates. *Phys. Chem. Chem. Phys.,* 2016, **18**, 14840.

[15] F. May, V. Marcon, M. R. Hansen, F. Grozema, D. Andrienko, Relationship Between Supramolecular Assembly and Charge-Carrier Mobility in Perylenediimide Derivatives: the Impact of Side Chains. *J. Mater. Chem.,* 2011, **21**, 9538.

[16] (a) S. H. Kim, J. R. Parquette. A Model for the Controlled Assembly of Semiconductor Peptides. *Nanoscale*, 2012, **4**, 6940. (b) J. D. Tovar. Supramolecular Construction of Optoelectronic Biomaterials. *Acc. Chem. Res.*, 2013, **46**, 11527. (c) A. Das, S. Ghosh. H-bonding Directed Programmed Supramolecular Assembly of Naphthalene-Diimide (NDI) Derivatives. *Chem. Commun.*, 2016, **52**, 6860.

[17] R. Marty, R. Szilluweit, A. Sánchez-Ferrer, S. Bolisetty, J. Adamcik, R. Mezzenga, E.-C. Spitzner, M. Feifer, S. N. Steinmann, C. Corminboeuf, H. Frauenrath, Hierarchically Structured Microfibers of "Single Stack" Perylene Bisimide and Quaterthiophene Nanowires. *ACS Nano,* 2013, **7**, 8498.

[18] L. Wang, Q. Li, Z. Shuai, L. Chen, Q. Shi, Multiscale Study of Charge Mobility of Organic Semiconductor with Dynamic Disorders. *Phys. Chem. Chem. Phys.,* 2010, **12**, 3309.

[19] M. Schrader, R. Fitzner, M. Hein, C. Elschner, B. Baumeier, K. Leo, M. Riede, P. Bäuerle, D. Andrienko, Comparative Study of Microscopic Charge Dynamics in Crystalline Acceptor-Substituted Oligothiophenes. *J. Am. Chem. Soc.,* 2012, **134**, 6052.

[20] T. Okamoto, K. Nakahara, A. Saeki, S. Seki, J. H. Oh, H. B. Akkerman Z. Bao, Y. Matsuo, Aryl-Perfluoroaryl Substituted Tetracene: Induction of Face-to-Face π-π Stacking and Enhancement of Charge Carrier Properties. *Chem. Mater.*, 2011, **23**, 1646.

[21] (a) M.-X. Zhang, G.-J. Zhao, Modification of n-Type Organic Semiconductor Performance of Perylene Diimides by Substitution in Different Positions: Two-Dimensional π-Stacking and Hydrogen Bonding. *ChemSusChem*, 2012, **5**, 879. (b) S. Yagai, T. Seki, H. Murayama, Y. Wakikawa, T. Ikoma, Y. Kikkawa, T. Karatsu, A. Kitamura, Y. Honsho, S. Seki. Structural and Electronic Properties of Extremely Long Perylene Bisimide Nanofibers Formed through a Stoichiometrically Mismatched, Hydrogen-Bonded Complexation. *Small*, 2010, **6**, 2731.

[22] (a) D. A. Stone, A. S. Tayi, J. E. Goldberger, L. C. Palmer, S. I. Stupp, Self-Assembly and Conductivity of Hydrogen-Bonded Oligothiophene Nanofiber Networks. *Chem. Commun.,* 2011, **47**, 5702. (b) I. D. Tevis, L. C. Palmer, D. J. Herman, I. P. Murray, D. A. Stone, S. I. Stupp, Self-Assembly and Orientation of Hydrogen-Bonded Oligothiophene Polymorphs at Liquid-Membrane-Liquid Interfaces. *J. Am. Chem. Soc.,* 2011, **133**, 16486. (c) B. D. Wall, S. R. Diegelmann, S. Zhang, T. J. Dawidczyk, W L. Wilson, H. E. Katt, H.-Q. Mao, J. D. Tovar, Aligned Macroscopic Domains of Optoelectronic Nanostructures Prepared via Shear-Flow Assembly of Peptide Hydrogels. *Adv. Mater.,* 2011, **23**, 5009. (d) H. Liu, É. Brémond, A. Prlj, J. F. Gonthier, C. Corminboeuf, Adjusting the Local Arrangement of π-Stacked Oligothiophenes through Hydrogen Bonds: A Viable Route to Promote Charge Transfer. *J. Phys. Chem. Lett,*. 2014, **5**, 2320.

[23] (a) E. F. Valeev, V. Coropceanu, D. A. da Silva Filho, S. Salman, J.-L. Brédas, Effect of Electronic Polarization on Charge-Transport Parameters in Molecular Organic Semiconductors. *J. Am. Chem. Soc.,* 2006, **128**, 9882. (b) C. Sutton, J. S. Sears, V. Coropceanu, J.-L. Brédas, Understanding the Density Functional Dependence of DFT- Calculated Electronic Couplings in Organic Semiconductors. *J. Phys. Chem. Lett.,* 2013, **4**, 919.

[24] W.-Q. Deng, L. Sun, J.-D. Huang, S. Chai, S.-H. Wen, K.-L. Han, Quantitative Prediction of Charge Mobilities of π-Stacked Systems by First-Principles Simulation. *Nat. Prot.,* 2015, **10**, 632.

[25] W.-J. Chi, Z.-S. Li, The Theoretical Investigation on the 4-(4-Phenyl-4-a-naphthylbutadieny)-triphenylamine Derivatives as Hole Transporting Materials for Perovskite-type Solar Cells, *Phys*. *Chem*. *Chem*. *Phys*., 2015, **17**, 5991.

[26] (a) J. Kirkpatrick, V. Marcon, J. Nelson, K. Kremer, D. Andrienko, Charge Mobility of Discotic Mesophases: A Multiscale Quantum and Classical Study. *Phys. Rev. Lett.,* 2007, **98**, 227402. (b) D. Andrienko, J. Kirkpatrick, V. Marcon, J. Nelson, K. Kremer, Structure-Charge Mobility Relation for Hexabenzocoronene Derivatives. *Phys. Stat. Sol.,* 2008, **245**, 830.

[27] F. May, M. Al-Helwi, B. Baumeier, W. Kowalsky, E. Fuchs, C. Lennartz, D. Andrienko, Design Rules for Charge-Transport Efficient Host Materials for Phosphorescent Organic Light-Emitting Diodes. *J. Am. Chem. Soc.,* 2012, **134**, 13818.

[28] J. Idé, R. Méreau, L. Ducasse, F. Castet, Y. Olivier, N. Martinelli, J. Cornil, D. Beljonne, Supramolecular Organization and Charge Transport Properties of Self-Assembled π-π Stacks of Perylene Diimide Dyes. *J. Phys. Chem. B,* 2011, **115**, 5593.

[29] (a) R. A. Marcus, Electron Transfer Reactions In Chemistry. Theory And Experiment. *Rev. Mod. Phys.,* 1993, **65**, 599. (b) P. F. Barbara, T. J. Meyer, M. A. Ratner, Contemporary Issues in Electron Transfer Research. *J. Phys. Chem.,* 1996, **100**, 13148.

[30] (a) A. Troisi, Prediction of the Absolute Charge Mobility of Molecular Semiconductors: the Case of Rubrene. *Adv. Mater.,* 2007, **19**, 2000. (b) H. Kobayashi, N. Kobayashi, S. Hosoi, N. Koshitani, D. Murakami, R. Shirasawa, Y. Kudo, D. Hobara, Y. Tokita, M. Itabashi, Hopping and Band Mobilities of Pentacene, Rubrene, and 2,7-Dioctyl[1]benzothieno[3,2- *b*][1]benzothiophene (C8-BTBT) from First Principle Calculations. *J. Chem. Phys.,* 2013, **139**, 014707.

[31] I. Yavus, B. N. Martin, J. Park, K. N. Houk, Theoretical Study of the Molecular Ordering, Paracrystallinity, And Charge Mobilities of Oligomers in Different Crystalline Phases. *J. Am. Chem. Soc.,* 2015, **137**, 2856.

[32] K. Takimiya, I. Osaka, T. Mori, M. Nakano, Organic Semiconductors Based on [1]Benzothieno[3,2-*b*][1]benzothiophene Substructure. *Acc. Chem. Res.,* 2014, **47**, 1493.

[33] Y. C. Chang, Y. D. Chen, C. H. Chen, Y. S. Wen, J. T. Lin, H. Y. Chen, M. Y. Kuo, I. Chao, Crystal Engineering for π-π Stacking via Interaction between Electron-Rich and Electron-Deficient Heteroaromatics. *J. Org. Chem.,* 2008, **73**, 4608.

[34] (a) C. D. Sherrill, T. Takatani, E. G. Hohenstein, An Assessment of Theoretical Methods for Nonbonded Interactions: Comparison to Complete Basis Set Limit Coupled-Cluster Potential Energy Curves for the Benzene Dimer, the Methane Dimer, Benzene-Methane, and Benzene-H_2S. *J. Phys. Chem. A,* 2009, **113**, 10146. (b) T. Janowski, P. Pulay, High Accuracy Benchmark Calculations on the Benzene Dimer Potential Energy Surface. *Chem. Phys. Lett.,* 2007, **447**, 27.

[35] K. J. Thorley, C. Risko, On the Impact of Isomer Structure and Packing Disorder in Thienoacene Organic Semiconductors. *J. Mater. Chem. C,* 2016, **4**, 4040.

[36] According to the Eq. 1, the transport rate is directly proportional to the square of the effective transfer intergal. Whilst its functional dependence on the reorganisation energy is somewhat more complex, higher k_+ values are expected for species with lower λ_+.

[37] In a realistic nanofibril planarity of flexible cores can be potentially promoted by environment before the charge transfer occurs.

[38] J. A. Lehrman, H. Cui, W.-W. Tsai, T. J. Moyer, S. I. Stupp, Supramolecular Control of Self-Assembling Terthiophene–Peptide Conjugates Through The Amino Acid Side Chain. *Chem. Commun.,* 2012, **48**, 9711.

[39] Y. Liu, Sun, X. C.-a. Di, Y. Liu, C. Du, K. Lu, S. Ye, G. Yu, Hexathienoacene: Synthesis, Characterization, and Thin-Film Transistors. *Chem. Asian J.,* 2010, **5**, 1550. Measured OTFT mobility of pentathienoacene on untreated SiO_2/Si is equal to 0.0043 $cm^2V^{-1}s^{-1}$, of hexathienoacene – 0.0022 $cm^2V^{-1}s^{-1}$.

[40] A. Kubas, F. Hoffmann, A. Heck, H. Oberhofer, M. Elstner, Blumberger, J. Electronic Couplings for Molecular Charge Transfer: Benchmarking CDFT, FODFT, and FODFTB against High-Level ab initio Calculations. *J. Chem. Phys.,* 2014, **140**, 104105. The largest electronic coupling matrix elements, computed using SCS-CC2 method, are equal to 0.394 eV for tetracene and 0.382 eV for pentacene.

[41] See Figure S1 of the Supporting Information. Computed transfer integrals of the dimers at zero longitudinal shift and optimised intercore separation are 0.479 eV for PTA and 0.464 eV for HTA, 0.488 eV for PTA(O) and 0.477 eV for HTA(O).

[42] Charge penetration is a short-range (< 4Å) attractive electrostatic interaction that arises from the interactions of the electrons of one monomer with the nuclei of the other and increases with orbital overlap.

[43] E. G. Hohenstein, J. Duan, C. D. Sherrill, Origin of the Surprising Enhancement of Electrostatic Energies by Electron-Donating Substituents in Substituted Sandwich Benzene Dimers, *J. Am. Chem. Soc.,* 2011, **133**, 13244.

[44] M. A. Freitag, M. S. Gordon, J. H. Jensen, W. J. Stevens, Evaluation of Charge Penetration Between Distributed Multipolar Expansions, *J. Chem. Phys.,* 2000, **112**, 7300.

[45] P. W. Atkins, Physical Chemistry, 5th ed. Oxford University Press: Oxford, U.K. 1994.

[46] S.-H. Wen, A. Li, J. Song, W.-Q. Deng, K.-L. Han, W. A. Goddard, First-Principles Investigation of Anistropic Hole Mobilities in Organic Semiconductors. *J. Phys. Chem. B,* 2009, **113**, 8813.

[47] S. Pronk, S. Pall, R. Schulz, P. Larsson, P. Bjelkmar, R. Apostolov, M. R. Shirts, J. C. Smith, P. M. Kasson, D. van der Spoel, B., Hess, E. Lindahl, GROMACS 4.5 A Highthroughput and Highly Parallel Open Source Molecular Simulation Toolkit. *Bioinformatics,* 2013, **29**, 845.

[48] GROMACS 4.6.3 Online reference. http://manual.gromacs.org/archive/4.6.3/online.html (accessed Mar 27, 2016).

[49] J. Wang, R. M. Wolf, J. W. Caldwell, P. A. Kollman, D. A. Case, Development and Testing of a General Amber Force Field. *J. Comput. Chem.,* 2004, **25**, 1157.

[50] K. Lindorff-Larsen, S. Piana, K. Palmo, P. Maragakis, J. L. Klepeis, R. O. Dror, D. E. Shaw, Improved Side-chain Torsion Potentials for the Amber ff99SB Protein Force Field. *Proteins*, 2010, **78**, 1950.

[51] D. A. Case, V. Babin, J. T. Berryman, R. M. Betz, Q. Cai, D. S. Cerutti, T. E. Cheatham, III, T. A. Darden, R. E. Duke, H. Gohlke, A. W. Goetz, S. Gusarov, N. Homeyer, P. Janowski, J. Kaus, I. Kolossváry, A. Kovalenko, T. S. Lee, S. LeGrand, T. Luchko, R. Luo, B. Madej, K. M. Merz, F. Paesani, D. R. Roe, A. Roitberg, C. Sagui, R. Salomon-Ferrer, G. Seabra, C. L. Simmerling, W. Smith, J. Swails, R. C. Walker, J. Wang, R. M. Wolf, X. Wu, P. A. Kollman 2014, AMBER 2014, University of California, San Francisco.

[52] A. Jakalian, B. L. Bush, D. B. Jack, C. I. Bayly, Fast, Efficient Generation of High Quality Atomic Charges. AM1-BCC Model I. Method. *J. Comput. Chem*., 2000, **21**, 132.

[53] C. Caleman, P. J. van Maaren, M. Hong, J. S. Hub, L. T. Costa, D. van der Spoel, Force Field Benchmark of Organic Liquids Density, Enthalpy of Vaporization, Heat Capacities, Surface Tension, Isothermal Compressibility, Volumetric Expansion Coefficient, and Dielectric Constant. *J. Chem. Theor. Comput.,* 2012, **8**, 61.

[54] G. Bussi, D. Donadio, M. Parrinello, Canonical Sampling Through Velocity Rescaling. *J. Chem. Phys.* 2007, **126**, 014101.

[55] T. Darden, D. York, L. Pedersen, Particle Mesh Ewald An Nlog(N) Method for Ewald Sums in Large Systems. *J. Chem. Phys.,* 1993, **98**, 10089.

[56] H. J. C. Berendsen, J. P. M. Postma, W. F. v. Gunsteren, A. DiNola, J. R. Haak, Molecular Dynamics with Coupling to an External Bath. *J. Chem. Phys.,* 1984, **81**, 3684.

[57] Rühle, V. Lukyanov, A. May, F. Schrader, M. Vehoff, T. Kirkpatrick, J. Baumeier, B. Andrienko, D. Microscopic Simulations of Charge Transport in Disordered Organic Semiconductors, *J. Chem. Theory Comput.,* 2011, **7**, 3335.

[58] C. Poelking, M. Tietze, C. Elschner, S. Olthof, D. Hertel, B. Baumeier, F. Würthner, K. Meerholz, K. Leo, D. Andrienko, Impact of Mesoscale Order on Open-Circuit Voltage in Organic Solar Cells. *Nat. Mater.,* 2015, **14**, 434.

[59] J. Kirkpatrick, V. Marcon, K. Kremer, J. Nelson, D. Andrienko, Columnar Mesophases of Hexabenzocoronene Derivatives. II. Charge Carrier Mobility, *J. Chem. Phys.,* 2008, **129**, 094506.

[60] C. M. Breneman, K. B. Wiberg, Determining Atom-Centered Monopoles from Molecular Electrostatic Potentials. The Need for High Sampling Density in Formamide Conformational Analysis, *J. Comput. Chem.,* 1990, **11**, 361.

[61] **Gaussian 09, Revision D.01**, M. J. Frisch, G. W. Trucks, H. B. Schlegel, G. E. Scuseria, M. A. Robb, J. R. Cheeseman, G. Scalmani, V. Barone, B. Mennucci, G. A. Petersson, H. Nakatsuji, M. Caricato, X. Li, H. P. Hratchian, A. F. Izmaylov, J. Bloino, G. Zheng, J. L. Sonnenberg, M. Hada, M. Ehara, K. Toyota, R. Fukuda, J. Hasegawa, M. Ishida, T. Nakajima, Y. Honda, O. Kitao, H. Nakai, T. Vreven, J. A. Montgomery, Jr., J. E. Peralta, F. Ogliaro, M. Bearpark, J. J. Heyd, E. Brothers, K. N. Kudin, V. N. Staroverov, R. Kobayashi, J. Normand, K. Raghavachari, A. Rendell, J. C. Burant, S. S. Iyengar, J. Tomasi, M. Cossi, N. Rega, J. M. Millam, M. Klene, J. E. Knox, J. B. Cross, V. Bakken, C. Adamo, J. Jaramillo, R. Gomperts, R. E. Stratmann, O. Yazyev, A. J. Austin, R. Cammi, C. Pomelli, J. W. Ochterski, R. L. Martin, K. Morokuma, V. G. Zakrzewski, G. A. Voth, P. Salvador, J. J. Dannenberg, S. Dapprich, A. D. Daniels, Ö. Farkas, J. B. Foresman, J. V. Ortiz, J. Cioslowski, and D. J. Fox, Gaussian, Inc., Wallingford CT, 2009.

[62] B. T. Thole, Molecular Polarizabilities Calculated with a Modified Dipole Interaction, *Chem. Phys.,* 1981, **59**, 341.

[63] (a) P. Kordt, D. Andrienko, Modeling of Spatially Correlated Energetic Disorder in Organic Semiconductors, *J. Chem. Theory Comput.,* 2016, **12**, 36. (b) L. B. Schein, A. Tyunev, The Contribution of Energetic Disorder to Charge Transport in Molecularly Doped Polymers, *J. Phys. Chem. C,* 2008, **112**, 7295.

[64] J. Ridley, M. Zerner, An Intermediate Neglect of Differential Overlap Technique for Spectroscopy" Pyrrole and the Azines. *Theor. Chim. Acta (Berl.),* 1973, **32**, 111.

[65] J. Kirkpatrick, An Approximate Method for Calculating Transfer Integrals Based on the ZINDO Hamiltonian, *Int. J. Quantum Chem.,* 2008, **108**, 51.

[66] S. N. Steinmann, C. Corminboeuf, Comprehensive Benchmarking of a Density-Dependent Dispersion Correction. *J. Chem. Theory Comput.,* 2011, **7**, 3567.

[67] **QChem 4.0**, Y. Shao, Z. Gan, E. Epifanovsky, A. T. B. Gilbert, M. Wormit, J. Kussmann, A. W. Lange, A. Behn, J. Deng, X. Feng, D. Ghosh, M. Goldey P. R. Horn, L. D. Jacobson, I. Kaliman, R. Z. Khaliullin, T. Kús, A. Landau, J. Liu, E. I. Proynov, Y. M. Rhee, R. M. Richard, M. A. Rohrdanz, R. P. Steele, E. J. Sundstrom, H. L. Woodcock III, P. M. Zimmerman, D. Zuev, B. Albrecht, E. Alguire, B. Austin, G. J. O. Beran, Y. A. Bernard, E. Berquist, K. Brandhorst, K. B. Bravaya, S. T. Brown, D. Casanova, C.-M. Chang, Y. Chen, S. H. Chien, K. D. Closser, D. L. Crittenden, M. Diedenhofen, R. A. DiStasio Jr., H. Dop, A. D. Dutoi, R. G. Edgar, S. Fatehi, L. Fusti-Molnar, A. Ghysels, A. Golubeva-Zadorozhnaya, J. Gomes, M. W. D. Hanson-Heine, P. H. P. Harbach, A. W. Hauser, E. G. Hohenstein, Z. C. Holden, T.-C. Jagau, H. Ji, B. Kaduk, K. Khistyaev, J. Kim, J. Kim, R. A. King, P. Klunzinger, D. Kosenkov, T. Kowalczyk, C. M. Krauter, K. U. Lao, A. Laurent, K. V. Lawler, S. V. Levchenko, C. Y. Lin, F. Liu, E. Livshits, R. C. Lochan, A. Luenser, P. Manohar, S. F. Manzer, S.-P. Mao, N. Mardirossian, A. V. Marenich, S. A. Maurer, N. J. Mayhall, C. M. Oana, R. Olivares-Amaya, D. P. O'Neill, J. A. Parkhill, T. M. Perrine, R. Peverati, P. A. Pieniazek, A. Prociuk, D. R. Rehn, E. Rosta, N. J. Russ, N. Sergueev, S. M. Sharada, S. Sharmaa, D. W. Small, A. Sodt, T. Stein, D. Stück, Y.-C. Su, A. J. W. Thom, T. Tsuchimochi, L. Vogt, O. Vydrov, T. Wang, M. A. Watson, J. Wenzel, A. White, C. F. Williams, V. Vanovschi, S. Yeganeh, S. R. Yost, Z.-Q. You, I. Y. Zhang, X. Zhang, Y. Zhou, B. R. Brooks, G. K. L. Chan, D. M. Chipman, C. J. Cramer, W. A. Goddard III, M. S. Gordon, W. J. Hehre, A. Klamt, H. F. Schaefer III, M. W. Schmidt, C. D. Sherrill, D. G. Truhlar, A. Warshel, X. Xua, A. Aspuru-Guzik, R. Baer, A. T. Bell,

N. A. Besley, J.-D. Chai, A. Dreuw, B. D. Dunietz, T. R. Furlani, S. R. Gwaltney, C.-P. Hsu, Y. Jung, J. Kong, D. S. Lambrecht, W. Liang, C. Ochsenfeld, V. A. Rassolov, L. V. Slipchenko, J. E. Subotnik, T. Van Voorhis, J. M. Herbert, A. I. Krylov, P. M. W. Gill, M. Head-Gordon. Advances in Molecular Quantum Chemistry Contained in The Q-Chem 4 Program Package. *Mol. Phys.* 2015, **113**, 184.

[68] (a) C. Adamo, V. Barone, Toward Reliable Density Functional Methods without Adjustable Parameters The PBE0 Model. *J. Chem. Phys.,* 1999, **110**, 6158. (b) S. N. Steinmann, C. Piemontesi, A. Delacht, C. Corminboeuf, Why are the Interaction Energies of Charge-Transfer Complexes Challenging for DFT*? J. Chem. Theory Comput.,* 2012, **8**, 1629. (c) S. N. Steinmann, C. Corminboeuf, Exploring the Limits of Density Functional Approximations for Interaction Energies of Molecular Precursors to Organic Electronics. *J. Chem. Theory Comput.,* 2012, **8**, 4305.

[69] **ADF2014**, SCM, Theoretical Chemistry, Vrije Universiteit, Amsterdam, The Netherlands, http://www.scm.com. E. J. Baerends, T. Ziegler, J. Autschbach, D. Bashford, A. Bérces, F. M. Bickelhaupt, C. Bo, P. M. Boerrigter, L. Cavallo, D. P. Chong, L. Deng, R. M. Dickson, D. E. Ellis, M. van Faassen, L. Fan, T. H. Fischer, C. Fonseca Guerra, M. Franchini, A. Ghysels, A. Giammona, S. J. A. van Gisbergen, A. W. Götz, J. A. Groeneveld, O. V. Gritsenko, M. Grüning, S. Gusarov, F. E. Harris, P. van den Hoek, C. R. Jacob, H. Jacobsen, L. Jensen, J. W. Kaminski, G. van Kessel, F. Kootstra, A. Kovalenko, M. V. Krykunov, E. van Lenthe, D. A. McCormack, A. Michalak, M. Mitoraj, S. M. Morton, J. Neugebauer, V. P. Nicu, L. Noodleman, V. P. Osinga, S. Patchkovskii, M. Pavanello, P. H. T. Philipsen, D. Post, C. C. Pye, W. Ravenek, J. I. Rodríguez, P. Ros, P. R. T. Schipper, G. Schreckenbach, J. S. Seldenthuis, M. Seth, J. G. Snijders, M. Solà, M. Swart, D. Swerhone, G. te Velde, P. Vernooijs, L. Versluis, L. Visscher, O. Visser, F. Wang, T. A. Wesolowski, E. M. van Wezenbeek, G. Wiesenekker, S. K. Wolff, T. K. Woo, A. L. Yakovlev.

[70] P. de Silva, C. Corminboeuf, Simultaneous Visualization of Covalent and Non-Covalent Interactions Using Regions of Density Overlap. *J. Chem. Theory Comput.,* 2014, **10**, 3745.

[71] M. Kohout. **DGrid, Version 4.6**, 2011, Radebeul.

[72] B. Jeziorski, R. Moszynski, K. Szalewicz, Perturbation Theory Approach to Intermolecular Potential Energy Surfaces of van der Waals Complexes, *Chem. Rev.,* 1994, **94**, 1887.

[73] A. J. Stone, M. Alderton, Distributed Multipole Analysis, *Mol. Phys.,* 1985, **56**, 1047.